Thermal Modeling and Experimental Validation in the LENS™ Process

Liang Wang[1], Sergio D. Felicelli[2], James E. Craig[3]

1. Center for Advanced Vehicular Systems, Mississippi State University, Mississippi State, MS 39762
2. Mechanical Engineering Department, Mississippi State University, Mississippi State, MS 39762
3. Stratonics, Inc., Laguna Hills, CA 92653

Reviewed, accepted August 23, 2007

Abstract

Several aspects of the thermal behavior of deposited stainless steel 410 (SS410) during the Laser Engineered Net Shaping (LENS™) process were investigated experimentally and numerically. Thermal images in the molten pool and surrounding area were recorded using a two-wavelength imaging pyrometer system, and analyzed using ThermaViz™ software to obtain the temperature distribution. The molten pool size, temperature gradient, and cooling rate were obtained from the recorded history of temperature profiles. The dynamic shape of the molten pool, including the pool size in both travel direction and depth direction, was investigated and the effect of different process parameters was illustrated. The thermal experiments were performed in a LENS™ 850 machine with a 3kW IPG laser for different process parameters. A three-dimensional finite element model was developed to calculate the temperature distribution in the LENS process as a function of time and process parameters. The modeling results showed good agreement with the experimental data.

Key words: Laser Engineered Net Shaping, LENS, rapid prototyping, thermal behavior

1. Introduction

Recent innovations in digital design and manufacturing of advanced materials and components have stimulated an important growth of the solid freeform fabrication technologies in modern industry. The Laser Engineered Net Shaping (LENS™) process is a particular example of these technologies that shows considerable potential for rapid manufacturing and repair applications. The LENS process utilizes a laser, metallic powder, and a computer aided design (CAD) solid model to fabricate three-dimensional fully dense and fully functional components [1-2]. It has been applied to fabricate components for a large class of metal alloys, such as low-alloy steels [3], stainless steel [4-5], nickel based alloys [6-7], and titanium alloys [8-9]. The advantage of the LENS process is to fabricate complex three dimensional components with high strength and ductility directly from a CAD solid model. The process can reduce the cost and time significantly through one-step operation. In order to achieve the rapid prototyping characteristics of the LENS process, several efforts have been made to investigate the influence of process parameters on the properties of the fabricated parts. The critical issues in the LENS process include the process repeatability, the geometry accuracy, and the uniformity of microstructure properties [10-12].

The main process parameters, such as laser power, travel velocity, and powder flow rate affect the temperature profile and cooling rate in the molten pool, as well as the thermal cycles at each location of the fabricated part. Consequently, they determine the size of the molten pool, the part deformation and the microstructure of the deposited layers. These, in turn, determine the geometry accuracy and the mechanical properties of the finished part. Therefore, the investigation of the thermal behavior in the LENS process, i.e., the history of temperature profiles, becomes essential to understand the process-property relationship and to provide fundamental insight for improvement of process control.

A number of studies have attempted to investigate the thermal behavior of the LENS process both experimentally and numerically. Two different types of thermal measurements have been employed, utilizing radiation pyrometers [13-18] and thermocouples [13-14]. Thermocouples were used for the temperature measurement away from the molten pool [13]. The thermal cycle as a function of time was obtained at each thermocouple location. Radiation pyrometry has been used for the temperature measurement inside and around the molten pool. Thermal images of the pool area were captured by a CCD camera, which was mounted outside the glove-box with an angle to the substrate plane [15, 18] or incorporated into the optical path of the laser [11, 12, 16, 17]. This measurement provides the peak temperature, temperature profile, temperature gradient and cooling rate in the molten pool, as well as the geometry of the molten pool based on the temperature distribution. It has been found that the laser power had the strongest influence on the molten pool temperature. As a result, process control based on the regulation of the laser power was adopted by implementing a closed loop control system. The comparison of temperature and size of the molten pool and geometry accuracy of the finished part, with and without closed loop control, has been studied [10-12, 16]. It has been found that the closed loop control can improve the geometry accuracy and microstructure uniformity of the finished part. The microstructure of the LENS-fabricated part is extremely complex because each location of the part experiences many thermal cycles before cooling down to the room temperature, which is not common in the traditional manufacturing process.

A complete information on the thermal behavior at each location of the part becomes essential in order to understand the mechanisms of the microstructure formation and the mechanical properties such as residual stress and hardness in the finished part. Numerical modeling can provide a complete temperature distribution in the LENS process and help in understanding the thermal histories. Some preliminary modeling studies can be found in the literature. Finite element models have been employed to predict the thermal behavior in the molten pool [19-20] and the molten pool size [21-23]. The thermal cycles for multi-layer deposition were predicted by modeling the LENS process for the single wall plate deposition [24-26].

Despite considerable progress to date, several key aspects of the process are still unclear, such as the temperature profile in the molten pool, the molten pool geometry for each layer as a function of the process parameters, and the overall spatial and temporal variation of the temperature field in the part. A careful calibration and validation of the thermal model is required in order to obtain reliable numerical predictions. The calibrated thermal model can then be coupled to a metallurgical model to predict the microstructure or to a mechanical model to predict the residual stress in the fabricated part.

In the present work, a two-wavelength imaging pyrometer was used to measure the temperature distribution in the molten pool and its surrounding area during the LENS deposition of a single wall plate of 410 type stainless steel (SS410). Different processing parameters, including laser power and travel velocity were used in studying the thermal behavior during the deposition. The variation of the molten pool geometry with the layer number was also investigated. A three-dimensional finite element model was developed to predict the temperature distribution and molten pool size as a function of time and process parameters. It showed a reasonable agreement between the calculated and measured results.

2. **Thermal Measurement**

A ThermaViz^{TM} two-wavelength imaging pyrometer system was used to capture thermal images of the molten pool and surrounding area. By using two-wavelength pyrometers, the temperature is determined from the ratio of the relative intensities of radiation at two different wavelengths, and independently of emissivity, thus providing a more accurate temperature measurement than one-wavelength systems. The acquired infrared images reflect the temperature distribution in and around the molten pool. According to Planck's law [12], the total radiation intensity is linked to the temperature of a black body and the radiation wavelength by the following equation:

$$E_\lambda = \frac{C_1}{\pi\lambda^5}\exp\left(\frac{-C_2}{\lambda T}\right) \tag{1}$$

where C_1 and C_2 are the Planck's constants. For the two-wavelength pyrometers, the ratio of intensity is given by

$$R = \frac{E_{\lambda_1}}{E_{\lambda_2}} = K_1 \exp\left(\frac{K_2}{T}\right) \tag{2}$$

where K_1 and K_2 are expressed as $K_1 = \left(\frac{\lambda_2}{\lambda_1}\right)^5$, and $K_2 = C_2\left(\frac{1}{\lambda_2} - \frac{1}{\lambda_1}\right)$, respectively.

The schematic and a side view of the thermal experimental setup are shown in Figures 1(a) and 1(b). The powder nozzles and laser assembly move in the x-y plane. When building a single-wall plate, after each pass, the substrate and the part move in the negative z direction. A digital Si-based CCD camera was mounted outside the glovebox at an angle of approximately 15° with the x-y plane so that a side view of the molten pool can be captured. The camera does not move during the LENS process so that it can capture the same Field Of View (FOV) all the time. The FOV was set to 22.0 mm by 25.0 mm in the horizontal and vertical directions, respectively. Optical magnification provides a spatial resolution of 20 μm/pixel. The long band selected was from 800 nm to 900 nm, and the short band from 700 nm to 800 nm. The imaging pyrometer records a dynamic range from 1450°C to 1860°C. The camera captures one frame every 2 seconds, then digitizes colored images and passes the frame data, including two wavelength intensity images, and temperature images to a personal computer for storage. ThermaViz^{TM} image analysis software was used to carry out further image post-processing.

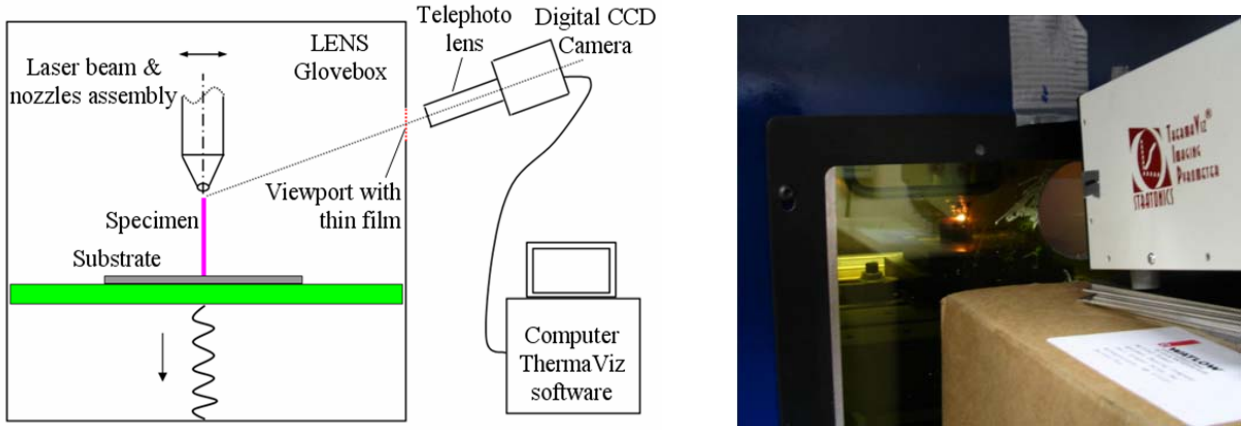

(a) (b)

Figure 1 - (a) Schematic and (b) side view of thermal experimental setup

Some factors such as the metallic vapor and hot air above the molten pool, metallic powder, and laser radiation, may distort the thermal images. A near-infrared filter is selected and installed between the iris and the camera in order to eliminate the image noise from those factors. A thin plastic film was added at the viewport of the optical path in order to keep the atmosphere in the glovebox separated from the outside environment, as shown in Figure 1(a). The camera, lens, filter, and thin-film were calibrated for temperature measurement with a standard tungsten filament source obtained from the National Institute of Standards and Technology. A model was developed to describe the relationship between the measured temperature and the ratio of the long wavelength to short wavelength intensities. The results from the model were compared with the calibration results using the standard tungsten filament source with and without the thin-film, and a good agreement can be found, as shown in Figure 2.

3. Thermal Modeling

A three dimensional finite element model was developed using the welding software SYSWELD. The model was used to predict the temperature distribution during the LENS deposition of a 10-layer single wall plate of SS410. The structure was built by overlapping 10 single tracks of material, each with a length of 10.0 mm, a thickness of 0.5 mm, and a width of 1.0 mm. The plate was deposited on the surface of a substrate having 5 mm thick, 10 mm wide, and 20 mm long. The temperature-dependent thermal properties of SS410 were employed, e.g. density, thermal conductivity, and specific heat, obtained from the SYSWELD database. It was assumed that the substrate material is initially at room temperature. A fixed temperature boundary condition equal to the room temperature is prescribed on the bottom surface of the substrate. The boundary conditions for all other surfaces take into account both laser heating and heat losses due to surface convection and radiation. The laser beam power is modeled as a Gaussian profile with a conical shape. The laser beam moves from one side to another in the same direction for each layer. More specific information about the geometry, meshing, and thermal properties can be found in Ref. [26]. The laser travel velocity is set at 2.5 mm/s and the laser power is 600 W. The process time for each layer is 10s, which is the same as that in the

experiments where the plate is 25 mm long. Because the modeled part is only 10 mm long, the laser takes 4s to deposit each layer. Therefore, an idle time of 6s during layer transition is selected in order to match the 10 s process time of the experiment. The modeling of a sample shorter than the experimental one is justified since the heating effect of the laser during deposition extends only to the immediate vicinity of the pool [26].

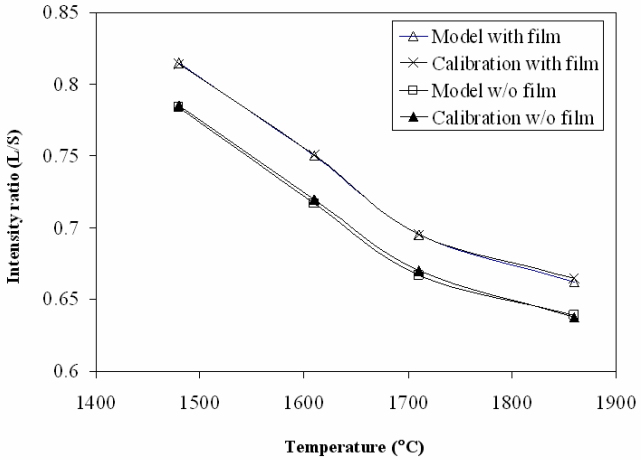

Figure 2 - Calibration curves for the ThermaViz™ two-wavelength thermal imaging pyrometer with and without film

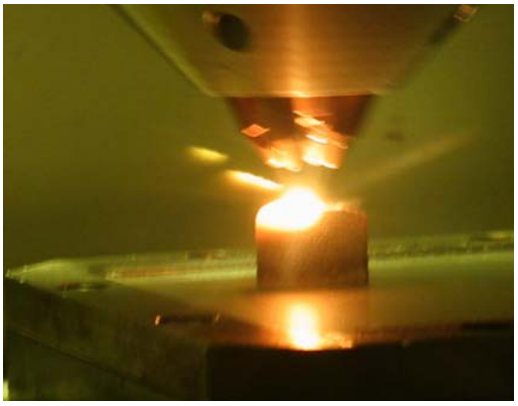

Figure 3 - Photograph of performing a single wall build during the LENS process

4. Results and Discussion

A series of LENS thermal experiments were performed on the LENS™ 850M and using 410 type stainless steel (SS410) powder with a 3kW IPG laser. The temperature measurements surrounding the molten pool area were performed for 9 samples with different laser powers and travel velocities by using the ThermaViz CCD camera. The process parameters for each sample are listed in Table 1.

Table 1 - Process parameters for each specimen in the LENS thermal experiments

Specimen No.	Laser power (W)	No. of Layers	Laser speed (mm/s)	Length of part (mm)	Powder flow rate (g/min)
4	300	25	2.5	25.4	0.6
5	300	25	4.2	25.4	0.8
7	300	50	8.5	38.1	1.4
8	600	25	2.5	25.4	0.6
9	600	25	4.2	25.4	0.7
10	600	50	8.5	38.1	1.4
11	450	25	2.5	25.4	0.6
12	450	25	4.2	25.4	0.8
13	450	50	8.5	38.1	1.3

A typical photograph of performing a single wall build during the LENS deposition is shown in Figure 3. Several photographs for typical specimens are shown in Figures 4(a) and 4(b). A uniform width of the single wall plate was obtained, as shown in the side view images in Figure

4. The process parameters used in Figures 4(a) and 4(b) were a laser power of 300 W with a laser travel velocity of 2.5 mm/s, and a laser power of 600 W with a laser travel velocity of 4.2 mm/s, respectively. It can be seen that the sample for higher laser power (600 W) is much thicker than that for lower laser power (300 W). This is because more powder is melted and solidified for each layer at higher laser power.

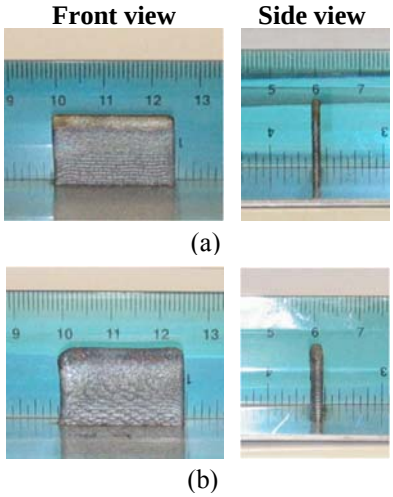

Figure 4 - Photograph of specimen samples
(a) P=300W, V=2.5mm/s
(b) P=600W, V=4.2mm/s

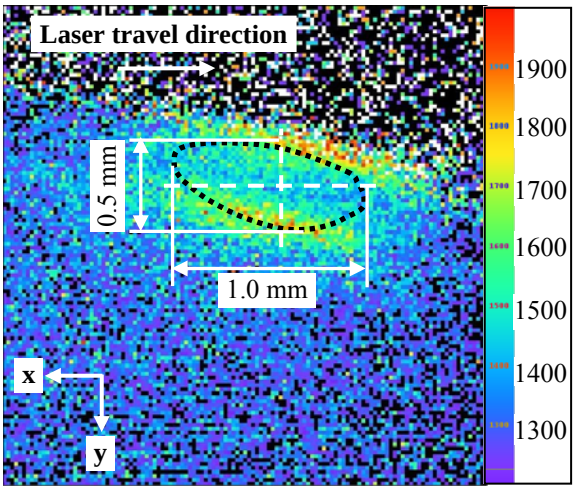

Figure 5 - Thermal image and molten pool size at P = 600W, V = 2.5 mm/s

Figure 5 shows the in-situ thermal image in and around the molten pool area of the part obtained with laser power of 600 W and travel velocity of 2.5mm/s. The temperature of each pixel in the thermal image was obtained from the intensity ratio of two different wavelengths. The shape of the molten pool, indicated by dashed lines, is determined by the isotherm corresponding to the melting temperature of SS410 (1450 °C). The molten pool size is approximately 1.0mm long and 0.5mm wide. In this image, x direction is defined as the opposite travel direction of the laser, and y direction is defined as the depth direction towards the substrate. The maximum temperature inside the molten pool is approximately 1650 °C. The region of high temperature observed outside the pool area corresponds to a slight misalignment of the two intensity images of the sensor and should be neglected.

Figures 6 and 7 show the temperature profiles and temperature gradients along the x and y centerlines of the pool, as shown in the image of Figure 5, respectively. The temperature at each location was obtained by using the average value of an 8×8 pixel square region in order to avoid the temperature fluctuation for each pixel. The maximum temperature in along these pathlines is 1627°C. For the x direction, the maximum temperature gradient can reach to 400 °C/mm, as shown in Figure 6(b), which occurs in the liquid-solid interface. For the y direction, the maximum temperature gradient is approximately 1000°C/mm, as shown in Figure 7(b), which is much higher than that in the x direction. This indicates that heat is dissipated much faster in the depth direction than in the travel direction due to the substrate heat sink. The cooling rates at the liquid-solid interface, derived from the temperature gradient and the laser travel velocity, vary between 1000 °C/s and 2500 °C/s.

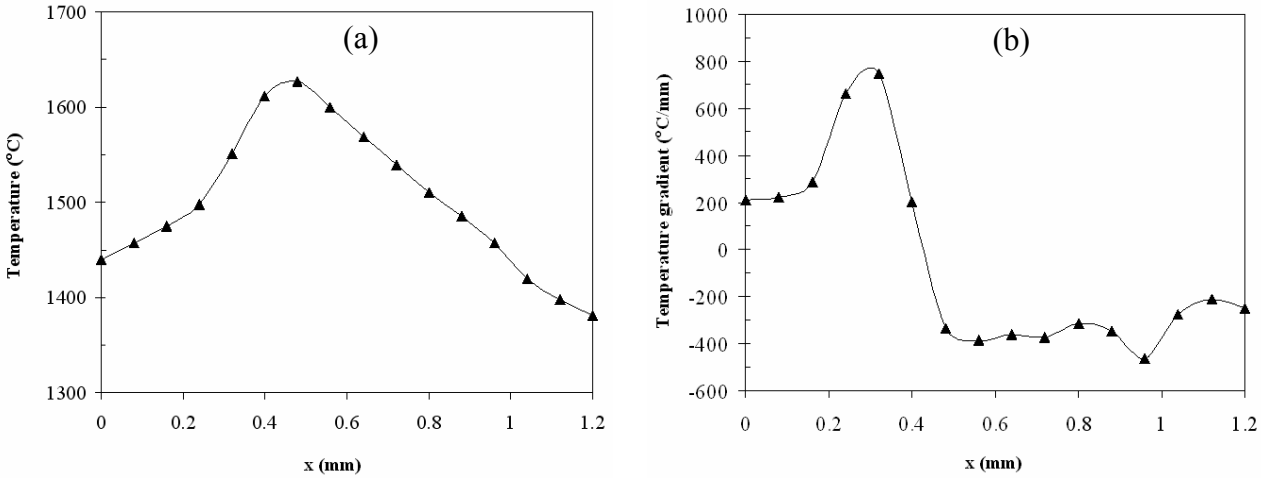

Figure 6 - (a) Temperature and (b) temperature gradient along the opposite travel direction (horizontal line x-direction in the image of Figure 5) for P = 600W, V = 2.5mm/s

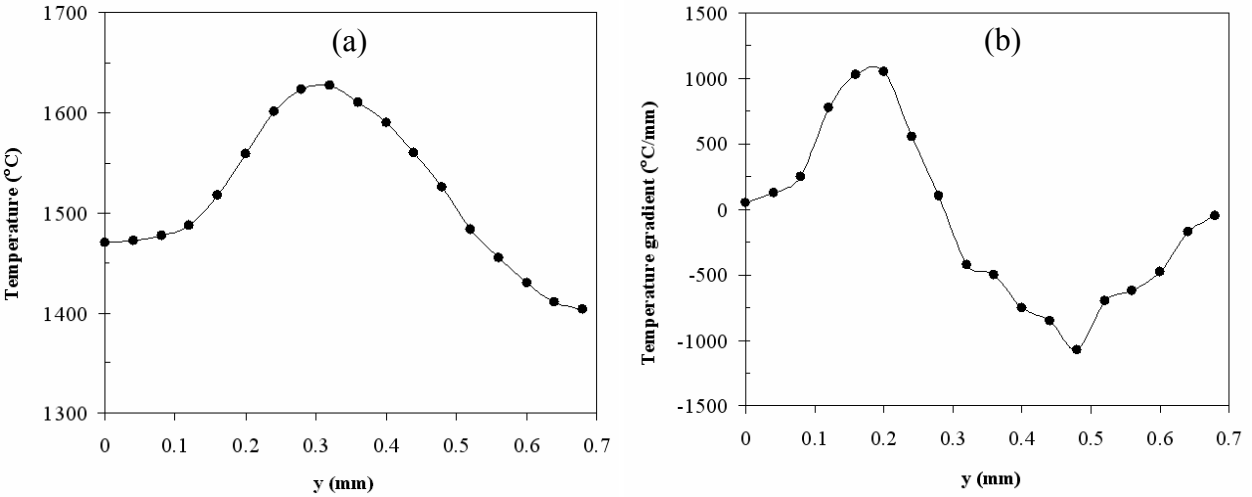

Figure 7 - (a) Temperature and (b) temperature gradient along the depth direction (vertical line y direction in the image of Figure 5) for P = 600W, V = 2.5mm/s

Figure 8 shows the temperature profiles along the x and y centerline from the center of the molten pool as a function of laser power for a travel velocity of 2.5mm/s. Both the molten pool size and the maximum temperature in the molten pool increase with laser power. The temperature profiles and temperature gradient outside the molten pool are similar for different laser powers. The maximum temperature in the molten pool reveals that the liquid is significantly superheated. Figure 9 shows the maximum temperature in the molten pool as a function of laser power and travel velocity. The maximum temperatures in the molten pool are in the range of 1500 °C to 1650 °C under the experimental conditions. It can be seen that the maximum temperature in the molten pool increases with increasing laser power and decreasing laser travel velocity. Lower travel velocity results in more heat input at each powder melting location, which increases the maximum temperature in the molten pool. However, the effects of the travel velocity on the maximum temperature in the molten pool are not significant.

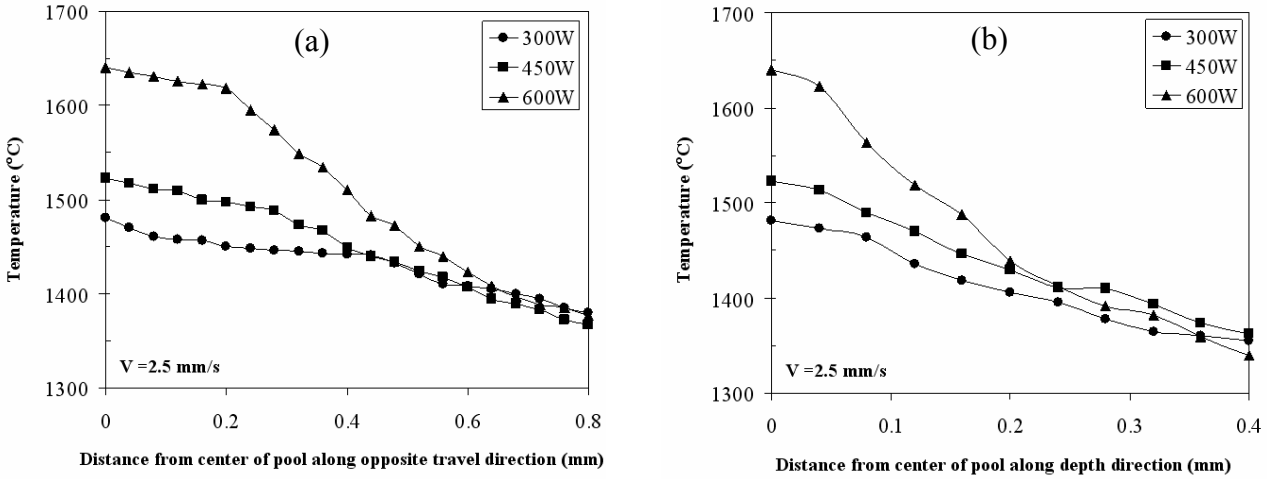

Figure 8 - Thermal profiles in the molten pool along (a) opposite travel directions, and (b) depth for different laser powers and a travel velocity of 2.5 mm/s.

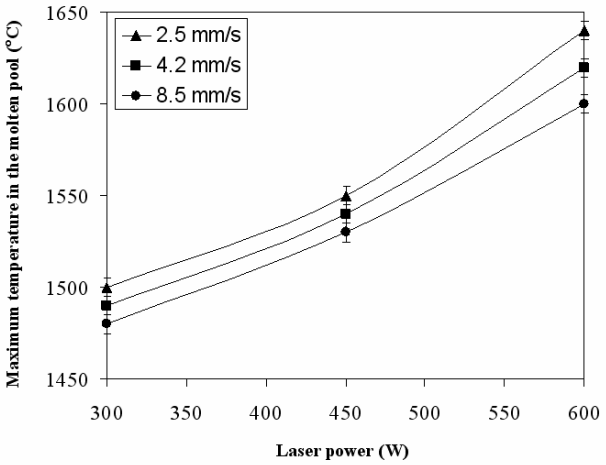

Figure 9 - Maximum temperatures in the molten pool versus laser powers for different laser travel velocities

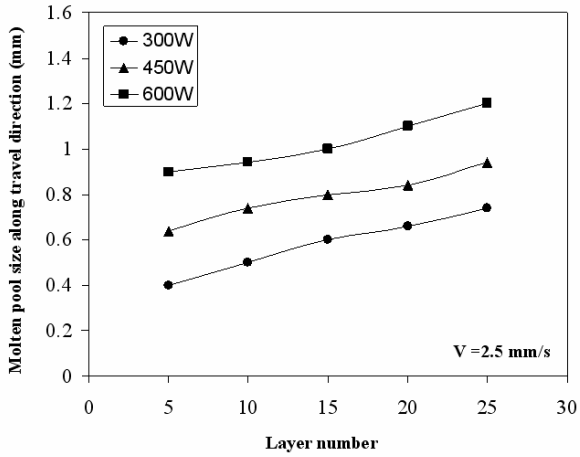

Figure 10 - Molten pool size along the laser opposite travel direction for different laser powers at travel velocity of 2.5 mm/s.

The molten pool geometry was investigated for different laser powers and travel velocities, as shown in Figures 10 and 11. Figure 10 presents the molten pool size along travel direction (x direction) for different laser powers at the travel velocity of 2.5 mm/s. For each case, the laser power is constant, and the molten pool size along x direction increases with the layer number. This is due to the substrate effect as a heat sink. It indicates that the closed-loop molten pool size control is necessary in order to produce uniform microstructure and accurate geometry of finished part. The maximum molten pool size is approximately 1.2mm at 600W and the minimum size is approximately 0.4 mm at 300W. Figure 11 shows the molten pool size along the depth direction (y direction) as a function of laser power and travel velocity. The molten pool size along y direction does not change much for different layers. It increases with the laser power and slightly increases with the travel velocity. The maximum cooling rate at the liquid-solid interface was investigated as a function of laser power and travel velocity, as shown in Figure 12. The maximum cooling rate increases with the travel velocity and decreases with the laser power.

The highest cooling rate is around 6000 °C/s at the lowest power (300 W) and the highest travel velocity (8.5 mm/s).

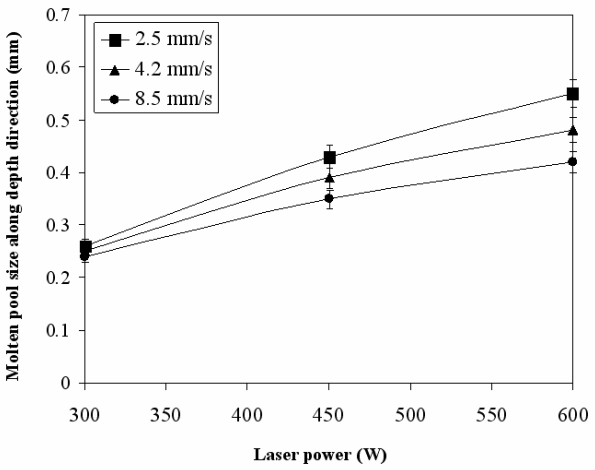

Figure 11 - Molten pool sizes along the depth direction versus laser powers for different laser travel velocities

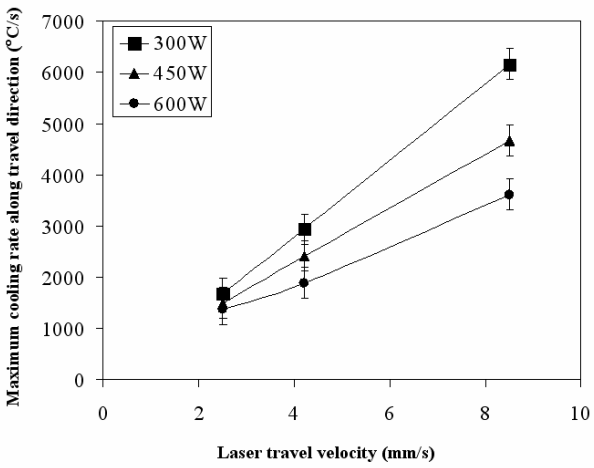

Figure 12 - Maximum cooling rates along the laser opposite travel direction versus laser travel velocities for different laser powers.

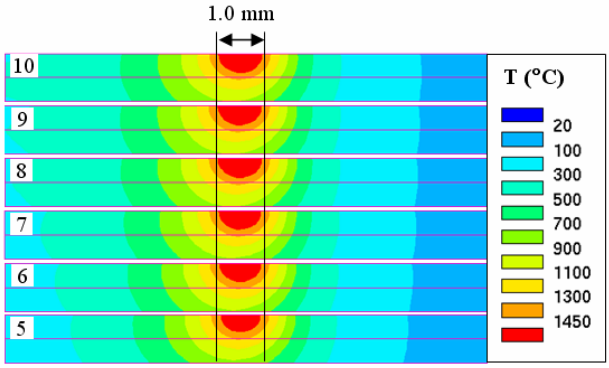

Figure 13 - Molten pool size distribution for each layer at P=600W, V=2.5mm/s calculated by finite element model

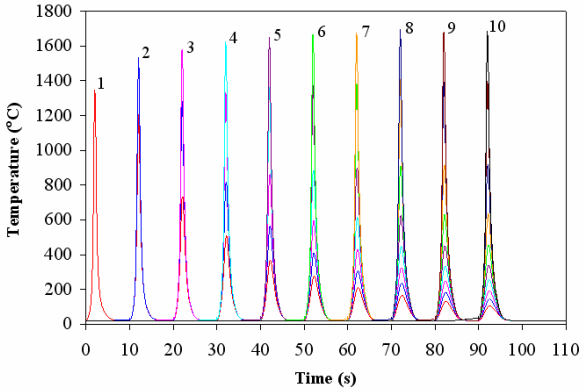

Figure 14 - Thermal cycles at the center of each layer at P=600W, V=2.5mm/s calculated by finite element model

The developed finite element model was used to calculate the molten pool size distribution for layers 5 to 10 at a laser power of 600 W and a travel velocity of 2.5 mm/s, as shown in Figure 13. The calculated average molten pool size is 1.0 mm, which is consistent with the experimental results. The size of the pool does not increase with layer number as much as observed in the experiment because of the longer idle time used in the model, giving the layer more time to cool down before the next layer deposition. The thermal cycles at the center of each layer is shown in Figure 14. The temperature at each location reaches the maximum point above the melting temperature when the laser beam moves over the point. After the laser beam passes by, the temperature quickly cools down to room temperature. The maximum temperature at the layer is similar after the fourth layer, where the substrate effects become negligible. The maximum temperature is approximately 1600 °C, which is consistent with the experimental results. Figure

15 shows the comparison between the modeling and experimental results for thermal profiles in the molten pool at the laser power 600 W and the travel velocity 2.5 mm/s. It shows a good agreement both for the depth direction and opposite travel direction.

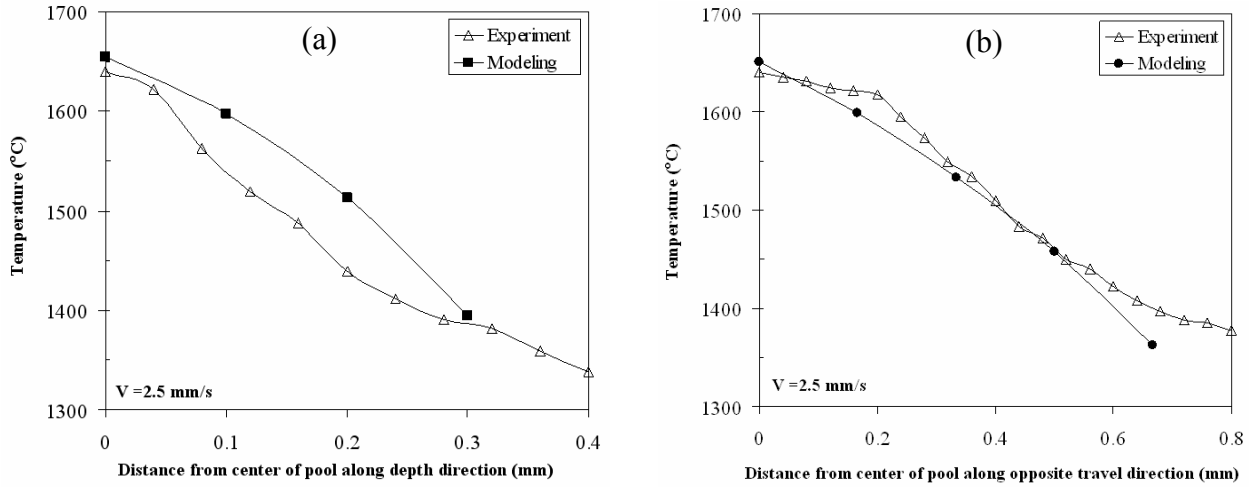

Figure 15 - Comparison between modeling and experimental results for thermal profiles in the molten pool along (a) depth and (b) opposite travel directions at P=600W, V=2.5mm/s

5. Conclusions

In this article, the thermal behavior of the LENS process for SS410 single wall build was characterized by using a two-wavelength imaging pyrometer. The experiments were performed in a LENS 850 machine with a 3kW IPG laser for different process parameters. The temperature distribution in the molten pool and the molten pool size were investigated. It was found that the maximum temperature in the molten pool is approximately 1600°C. The molten pool size is approximately 1.0 mm, and the maximum cooling rate in the liquid-solid interface is in the order of 10^3 °C/s. The molten pool size and cooling rate significantly depend on the travel velocity and the laser power. The thermal measurements give interesting and useful information when averaging is applied; however, there is a significant fluctuation in temperature readings at the pixel level. More accurate pyrometer performance would be desirable in order to confirm the present measurements. Numerical analysis using a three-dimensional finite element method shows good capability to predict the temperature distribution and molten pool size. A good agreement between the experimental and numerical results was obtained for molten pool size and temperature distribution in the molten pool. The thermal model can be used to understand the effects of the process parameters on the thermal cycles and thermal behavior. The model can also be applied to in-situ evaluation and monitoring by calculating the molten pool size, temperature distribution and cooling rate, for different process parameters.

Acknowledgements

The authors appreciate the sponsorship of the U.S. Army TACOM and the Center for Advanced Vehicular Systems (CAVS). The helpful assistance by Mr. David Baker of CAVS and Mr. Jim Bullen of Optomec Co during the experiments is gratefully acknowledged.

References

1. C. L. Atwood, M. L. Griffith, M E. Schlienger, L. D. Harwell, M. T. Ensz, D. M. Keicher, M. E. Schlienger, J. A. Romero, J. E. Smugeresky, "Laser Engineered Net Shaping (LENS®): A Tool for Direct Fabrication of Metal Parts", *Proceedings of ICALEO '98*, November 16-19, 1998, Orlando, FL, p. E-1-E-7.
2. J. Mazumder, H. Qi, "Fabrication of 3-D Components by Laser Aided Direct Metal Deposition", Proceedings of SPIE - The International Society for Optical Engineering, Vol. 5706, Critical Review: Industrial Lasers and Applications, 2005, p. 38-59.
3. D.M. Keicher, W.D. Miller, J.E. Smugeresky, J.A. Romero, "Laser Engineered Net Shaping (LENS^{TM}): Beyond Rapid Prototyping to Direct Fabrication", TMS Annual Meeting, Hard Coatings Based on Borides, Carbides & Nitrides: Synthesis, Characterization & Application, 1998, p. 369-377.
4. J.A. Brooks, T.J. Headley, C.V. Robino, "Microstructures of Laser Deposited 304L Austenitic Stainless Steel", Materials Research Society Symposium – Proceedings, Vol. 625, 2000, p. 21-30.
5. J.A. Brooks, C.V. Robino, T.J. Headley, J.R. Michael, "Weld Solidification and Cracking Behavior of Free-machining Stainless Steel", *Welding Journal (Miami, Fl)* ,Vol. 82, n 3, March, 2003, p. 51/S-64/S.
6. W. Liu, J.N. Dupont, "In-situ Reactive Processing of Nickel Aluminides by Laser-engineered Net Shaping", *Metallurgical and Materials Transactions A: Physical Metallurgy and Materials Science*, Vol. 34 A, n 11, November, 2003, p. 2633-2641.
7. M.L. Griffith, M.T. Ensz, J.D. Puskar, C.V. Robino, J.A. Brooks, J.A. Philliber, J.E. Smugeresky, W.H. Hofmeister, "**U**nderstanding the Microstructure and Properties of Components Fabricated by Laser Engineered Net Shaping (LENS)", Vol. 625, 2000, p. 9-20.
8. S.M. Kelly, S.L. Kampe, C.R. Crowe, "Microstructural Study of Laser Formed Ti-6Al-4V", *Materials Research Society Symposium - Proceedings*, Vol. 625, 2000, p. 3-8.
9. S.M. Kelly, S.L. Kampe, "Microstructural Evolution in Laser-deposited Multilayer Ti-6Al-4V Builds: Part II. Thermal Modeling", *Metallurgical and Materials Transactions A: Physical Metallurgy and Materials Science,* Vol. 35 A, n 6, June, 2004, p. 1869-1879.
10. G. Bi, A. Gasser, K. Wissenbach, A. Drenker, R. Poprawe, "Characterization of the Process Control for the Direct Laser Metallic Powder Deposition", *Surface & Coatings Technology*, Vol. 201, 2006, p. 2676-2683.
11. D. Hu, H. Mei, and R. Kovacevic, "Improving Solid Freeform Fabrication by Laser-based Additive Manufacturing", Proceedings of The Institution of Mechanical Engineers, Part B: Journal of Engineering Manufacture, Vol. 216, 2002, p. 1253-1264.
12. D. Hu, and R. Kovacevic, "Modelling and Measuring the Thermal Behavior of the Molten Pool in Closed-loop Controlled Laser-based Additive Manufacturing", Proceedings of The Institution of Mechanical Engineers, Part B: Journal of Engineering Manufacture, Vol. 217, 2003, p. 441-452.
13. M. L. Griffith, M. E. Schlienger, L. D. Harwell, M. S. Oliver, M. D. Baldwin, M. T. Ensz, J. E. Smugeresky, M. Essien, J. Brooks, C. V. Robino, W. H. Hofmeister, M. J. Wert, D. V. Nelson, "Thermal behavior in the LENS^{TM} process", Proceedings of the Solid Freeform Fabrication Symposium, Austin, TX, 1998, p. 89-97.
14. M. L. Griffith, M. E. Schlienger, L. D. Harwell, M. S. Oliver, M. D. Baldwin, M. T. Ensz, J. E. Smugeresky, M. Essien, J. Brooks, C. V. Robino, W. H. Hofmeister, M. J. Wert, D. V.

Nelson, "Understanding thermal behavior in the LENS™ process", *Journal of Materials Design*, Vol. 20, 1999, p. 107-114.
15. W. Hofmeister, M. Wert, J. Smugeresky, J.A. Philliber, M. Griffith, and M. Ensz, "Investigation of solidification in the laser engineered net shaping (LENS™) process", *JOM*, Vol.51, 1999.
16. W. Hofmeister, D. MacCallum, and G. Knorovsky, "Video Monitoring and Control of the LENS Process", Ninth International Conference on Computer Technology in Welding, Detroit, MI, 1999, p. 187-196.
17. W. Hofmeister, M. Griffith, M. Ensz, J. Smugeresky, "Solidification in Direct Metal Deposition by LENS® Processing", JOM-Journal of the Minerals Metals & Materials Society, Vol. 53, n9, 2001, p. 30-34.
18. W. Wei, Y. Zhou, R. Ye, D. Lee, J.E. Craig, J.E. Smugeresky, and E.J. Lavernia, "Investigation of the Thermal Behavior during the LENS Process", International Conference on Metal Powder Deposition for Rapid Manufacturing, San Antonio, TX, 2002, p. 128-135.
19. R. Ye, J.E. Smugeresky, B. Zheng, Y. Zhou, E.J. Lavernia, 2006, "Numerical Modeling of the Thermal Behavior during the LENS process", *Material Science and Engineering A*, Vol. 428, p. 47-53.
20. L. Wang and S. Felicelli, "Analysis of Thermal Phenomena in LENS™ Deposition", *Materials Science and Engineering A*, Vol. 435-436, 2006, p. 625-631.
21. M. Labudovic, D. Hu, and R. Kovacevic, "A Three Dimensional Model for Direct Laser Metal Powder Deposition and Rapid Prototyping", *Journal of Materials Science*, Vol. 38, 2003, p. 35-49.
22. J. Beuth, A. Vasinonta, and M. Griffith, "Process Maps for Laser Deposition of Thin-Walled Structures", Proceedings of the Solid Freeform Fabrication Symposium, August, 1999, Austin, TX, p. 383-391.
23. A. Vasinonta, J. L. Beuth, M. L. Griffith, "A Process Map for Consistent Build Conditions in the Solid Freeform Fabrication of Thin-Walled Structures", *Journal of Manufacturing Science and Engineering*, Vol. 123, November 2001, p. 615-622.
24. L. Costa, R. Vilar, T. Reti, and A.M. Deus, "Rapid Tooling by Laser Powder Deposition: Process Simulation Using Finite Element Analysis", *Acta Materialia*, Vol. 53, 2005, p. 3987-3999.
25. L. Wang, S.D. Felicelli, Y. Gooroochurn, P.T. Wang, M.F. Horstemeyer, "Optimization of the LENS™ Process for Steady Molten Pool Size," *Materials Science and Engineering A,* 2007 (in press)
26. L. Wang, and S.D. Felicelli, "Process Modeling in Laser Deposition of Multilayer SS410 Steel," *Journal of Manufacturing Science and Engineering*, 2007 (in press)